International Journal of
Molecular Sciences

MDPI

Article

Comprehensive Simulation of Ca^{2+} Transients in the Continuum of Mouse Skeletal Muscle Fiber Types

Oscar A. Rincón [1,2], Andrés F. Milán [2], Juan C. Calderón [2] and Marco A. Giraldo [1,*]

[1] Biophysics Group, Institute of Physics, University of Antioquia, Medellín 050010, Colombia; oandres.rincon@udea.edu.co
[2] Physiology and Biochemistry Research Group-PHYSIS, Faculty of Medicine, University of Antioquia, Medellín 050010, Colombia; andres.milan@udea.edu.co (A.F.M.); jcalderonv00@yahoo.com (J.C.C.)
* Correspondence: mantonio.giraldo@udea.edu.co; Tel.: +57-3015440055

Abstract: Mag-Fluo-4 has revealed differences in the kinetics of the Ca^{2+} transients of mammalian fiber types (I, IIA, IIX, and IIB). We simulated the changes in $[Ca^{2+}]$ through the sarcomere of these four fiber types, considering classical (troponin –Tn–, parvalbumin –Pv–, adenosine triphosphate –ATP–, sarcoplasmic reticulum Ca^{2+} pump –SERCA–, and dye) and new (mitochondria –MITO–, Na^+/Ca^{2+} exchanger –NCX–, and store-operated calcium entry –SOCE–) Ca^{2+} binding sites, during single and tetanic stimulation. We found that during a single twitch, the sarcoplasmic peak $[Ca^{2+}]$ for fibers type IIB and IIX was around 16 μM, and for fibers type I and IIA reached 10–13 μM. The release rate in fibers type I, IIA, IIX, and IIB was 64.8, 153.6, 238.8, and 244.5 μM ms^{-1}, respectively. Both the pattern of change and the peak concentrations of the Ca^{2+}-bound species in the sarcoplasm (Tn, PV, ATP, and dye), the sarcolemma (NCX, SOCE), and the SR (SERCA) showed the order IIB $\geq$ IIX > IIA > I. The capacity of the NCX was 2.5, 1.3, 0.9, and 0.8% of the capacity of SERCA, for fibers type I, IIA, IIX, and IIB, respectively. MITO peak $[Ca^{2+}]$ ranged from 0.93 to 0.23 μM, in fibers type I and IIB, respectively, while intermediate values were obtained in fibers IIA and IIX. The latter numbers doubled during tetanic stimulation. In conclusion, we presented a comprehensive mathematical model of the excitation–contraction coupling that integrated most classical and novel Ca^{2+} handling mechanisms, overcoming the limitations of the fast- vs. slow-fibers dichotomy and the use of slow dyes.

Keywords: ECC; Ca^{2+} dyes; mathematical simulation; muscle cells; tetanus

Citation: Rincón, O.A.; Milán, A.F.; Calderón, J.C.; Giraldo, M.A. Comprehensive Simulation of Ca^{2+} Transients in the Continuum of Mouse Skeletal Muscle Fiber Types. *Int. J. Mol. Sci.* **2021**, *22*, 12378. https://doi.org/10.3390/ijms222212378

Academic Editor: Carlo Zancanaro

Received: 6 September 2021
Accepted: 12 October 2021
Published: 17 November 2021

1. Introduction

In mammalian skeletal muscle fibers, the action potentials (AP) lead to contractions mediated by the release of Ca^{2+} from the sarcoplasmic reticulum (SR), in a process known as excitation–contraction coupling (ECC) [1]. After release, the Ca^{2+} ions bind to a diversity of sites, which include troponin (Tn), parvalbumin (PV), and adenosine triphosphate (ATP). They also flow into the mitochondria (MITO) [1], before being transported back to the SR by a Ca^{2+} ATPase (SERCA). Small amounts of Ca^{2+} are transported outside the cell by the Na^+/Ca^{2+} exchanger (NCX). Store-operated Ca^{2+} entry (SOCE) allows Ca^{2+} enter the fiber through Orai1, as a response to the intra SR Ca^{2+} sensing function of the stromal interaction molecules (STIM) [2–4]. In fast twitch fibers, SOCE acts in a transient fast mode during an individual AP and after each AP in a train of stimulations [5].

Experiments in muscle fibers loaded with fluorescent indicators have revealed sizeable differences in the kinetic parameters of electrically elicited Ca^{2+} transients according to the continuum of fiber types [6]. These variances arise due to the differential quantity and kinetics of the proteins and organelles involved in Ca^{2+} handling present in the muscle fibers [1,6]. For instance, SERCA is more abundant in fast fibers [7,8], and PV is almost negligible in slow, but abundantly found in the fastest fibers [9].

Mathematical models that integrate information obtained on mammalian ECC under different experimental conditions have been used to simulate Ca^{2+} transients in both slow-twitch and fast-twitch fibers [10,11]. However, the nature of the fibers used has not always been doubtlessly established. Furthermore, a major limitation of several models is their dichotomic approach (slow and fast), yet there are experimentally measured Ca^{2+} transients of at least four fiber types: I, IIA, IIX, and IIB [6]. Some models have not included important mechanisms dealing with Ca^{2+}, such as the mitochondria or the NCX, despite their importance in shaping the Ca^{2+} transients in different fiber types [12,13].

A recent model of skeletal muscle ECC, interestingly included the MITO and proteins such as the mitochondrial Ca^{2+} uniporter (MCU) and the mitochondrial NCX (NCE) [14]. However, that model was performed based on Ca^{2+} transients' measurements with Fura-2, while the most suitable dyes to study ECC in skeletal muscle seem to be the low affinity, fast Ca^{2+} dyes, such as Mag-Fura-2 and Mag-Fluo-4 [1,15]. This explains why the reported amplitude of the signal (0.4 μM) was very low compared to previously published values being 10–20 μM in murine Flexor digitorum brevis (FDB) fibers with Mag-Fura-2 and Mag-Fluo-4 [15–17].

In this work, we used measurements carried out with the fast Ca^{2+} dye Mag-Fluo-4 and a theoretical model to estimate the Ca^{2+} movements produced during single and tetanic Ca^{2+} transients in the four murine skeletal muscle fiber types. This permitted us to make a simulated comparison of the Ca^{2+} movement across the four fiber types, including the variations in the mitochondrial $[Ca^{2+}]$, the NCX, the SOCE, and their influence on the sarcoplasmic Ca^{2+} regulation, and further overcoming the limitations imposed by slow Ca^{2+} dyes.

2. Results

Experimentally recorded, raw, single, and tetanic Mag-Fluo-4 Ca^{2+} transients were calibrated in order to obtain the $\Delta[Ca^{2+}]$ in the sarcoplasm (Figure 1). The $[Ca^{2+}]$ peaks for the continuum of fiber types were: IIB and IIX: 16.58 μM, IIA: 12.77 μM, and I: 10.13 μM (Figure 1A). For the tetanic Ca^{2+} transients, subsequent peaks were also calculated (I: 11.24, 12.95, 14.81, and 16.47 μM; IIB: 12.13, 12.29, 12.24, and 11.96 μM) (Figure 1B).

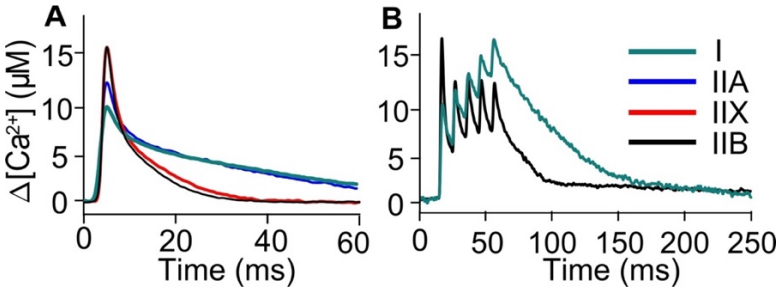

Figure 1. Experimental, calibrated measurements of $[Ca^{2+}]$ during Ca^{2+} transients elicited by a single and a train of AP (100 Hz) in mouse fibers at room temperature (21–23 °C). All fibers were classified by myosin heavy chain direct determination in the original paper. Fluorescence recordings generated with Mag-Fluo-4 were used to obtain the $\Delta[Ca^{2+}]$ in the sarcoplasm produced by a single AP in fiber types I (green), IIA (blue), IIX (red), and IIB (black) (**A**) and a train of 5 AP in fibers I and IIB (**B**).

These calibrated signals fed all next estimations and simulations, as described in the Methods section and Table 1. First, we mathematically estimated the release rate of Ca^{2+} (J_{Rel}) for both single and tetanic transients (Figure 2A,B; Table 2) and then simulated the Ca^{2+} kinetics in the sarcoplasm (Figure 2C,D), the SR (Figure 2E,F), and MITO (Figure 2G,H). Fibers type II peaked higher than fibers type I (~137% higher for IIA and 269–277% higher for IIX and IIB). The J_{Rel} estimated in tetanic Ca^{2+} transients shows that the last peak's amplitude is reduced over 10 times for type I fibers and up to 7 times for IIB, IIX, and IIA (Figure 2B; Table 2). The simulated sarcoplasmic $\Delta[Ca^{2+}]$ closely resembled the experimental recording described above. The $[Ca^{2+}]_{SR}$ rapidly decreased and slowly

recovered as expected. Although qualitatively similar for all fiber types, quantitative differences arose mainly between the fibers type I and all fibers type II, in agreement with the fact that the Ca^{2+} released by the fibers type I was the lowest.

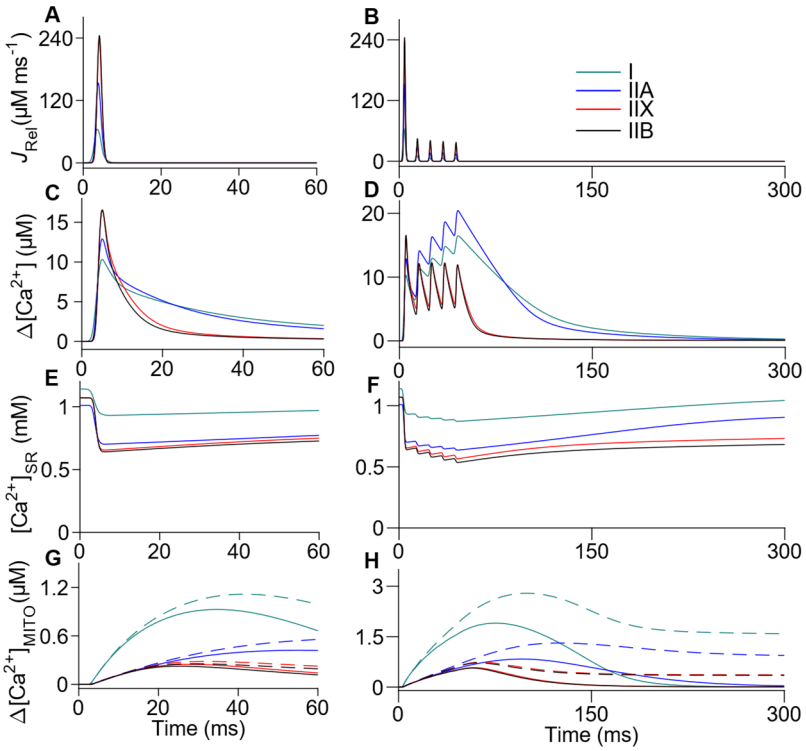

Figure 2. Simulation of release rate of Ca^{2+} and free [Ca^{2+}] in the three compartments of the model. The release rate of Ca^{2+} was estimated from the measurements of Δ[Ca^{2+}] in fibers I, IIA, IIX, and IIB (**A**). The model was used to reproduce the Δ[Ca^{2+}] obtained experimentally in the sarcoplasm (**C**,**D**) and to estimate the Δ[Ca^{2+}] in the SR (**E**,**F**), and MITO (**G**,**H**, solid line). The release rate of Ca^{2+} was used in the first AP of the tetanic Ca^{2+} transient simulation and in subsequent AP rescaled to match the experimental Δ[Ca^{2+}] peaks (**B**). The tetanic Ca^{2+} transient of IIA and IIX fibers were simulated assuming that they share morphology with I and IIB fibers, respectively. The total [Ca^{2+}] in MITO during the Ca^{2+} transients (**G**,**H**, dashed lines), was obtained from the sum of Δ[Ca^{2+}]$_{MITO}$ and the Ca^{2+} bound to B. MITO simulations were extended in time for the tetanic transients in the Figure S1, in order to show the return of [Ca^{2+}] to the basal levels.

There was a higher value in Δ[Ca^{2+}]$_{MITO}$ for the fibers type I (up to four times) as compared to the three fibers type II. The total [Ca^{2+}] in MITO, considering both forms, bound to B and free, achieves a peak value of 0.26–1.12 μM after a single AP and 0.72–2.8 μM after 5 AP. Regarding the SR compartment, our calculations show that the available Ca^{2+} is reduced up to ~63% (I: 82%, IIA: 63%, IIX: 64%, and IIB: 63%) for single transients, but to almost 53% (I: 76%, IIA: 63%, IIX: 56%, and IIB: 53%) after a train of five shocks (Figure 2E,F).

We also calculated the variations in [Ca^{2+}] for the buffers present in the three simulated compartments (Figure 3), for both single (left column) and tetanic transients (right column). The differences in [CaPV] show the PV buffer influence in the first part of [Ca^{2+}] decay obtained in the IIX and IIB fibers, compared with I and IIA fibers. The second part of the decay, when the sarcoplasmic [Ca^{2+}] is near steady state, was less affected by the PV buffering. The Δ[CaDye] and Δ[CaATP] simulations were not shown as they resemble the shape of the sarcoplasmic [Ca^{2+}] already shown (Figure 2C,D), but with different peaks (reported in Table 3). The Δ[CaDye] explains only 2.7% of the intracellular dye in the fiber type IIA and 2.2% in fiber types I, IIX, and IIB, thus ensuring dye unsaturation.

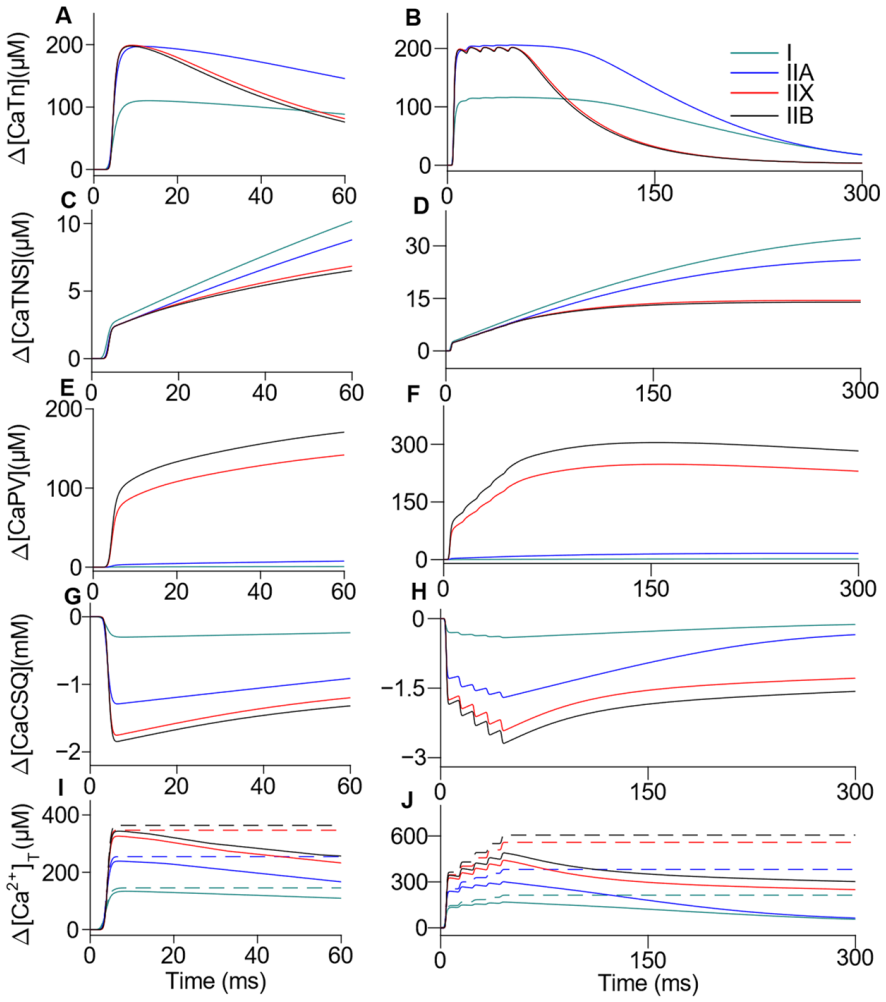

Figure 3. Simulation of single and tetanic Ca^{2+} transients buffering. The $\Delta[Ca^{2+}]$ coupled to the sarcoplasmic buffers: Tn (**A**,**B**), non-specific sites (TNS) (**C**,**D**), and PV (**E**,**F**); and the SR buffer: calsequestrin (CSQ) (**G**,**H**) is shown for single (left column) and tetanic (right column) transients. The total $[Ca^{2+}]$ in the sarcoplasm (solid line), was calculated as the sum of the $\Delta[Ca^{2+}]$ in both free and bound forms, whereas the total $[Ca^{2+}]$ released (dashed line), is the numerical integration of J_{Rel} (**I**,**J**).

Figure 4 shows that the $[Ca^{2+}]$ in the sarcoplasm is mainly recaptured by the SERCA. In general, the amount of Ca^{2+} handled by the NCX was 41–121 times lower after 1 AP and 34–88 times lower after 5 AP, compared to the SERCA capacity. Moreover, the rate of transport by NCX was notably reduced when the sarcoplasmic $[Ca^{2+}]$ achieves low values in IIX and IIB fibers given its low affinity. The SERCA pump maintains its influence in $[Ca^{2+}]$ regulation near resting conditions. The $[Ca^{2+}]$ returned to the sarcoplasm by the SOCE was negligible in all fibers compared to the total $[Ca^{2+}]$ released. The total $[Ca^{2+}]$ handled by each mechanism after the simulated time intervals, the free $[Ca^{2+}]$ reached in each compartment, and the Ca^{2+} bound to the chemical species are reported in Table 3. A longer time interval of the tetanic Ca^{2+} transient simulation was included for some reactions (Figure S1). The total amount of Ca^{2+} obtained at rest considering all compartments of the model, including the extracellular space, remained constant during the simulated activation interval. We obtained that the variations in the total amount of Ca^{2+} were lower than 10^{-6} μM. This result evidence that truncation errors were negligible during the simulations.

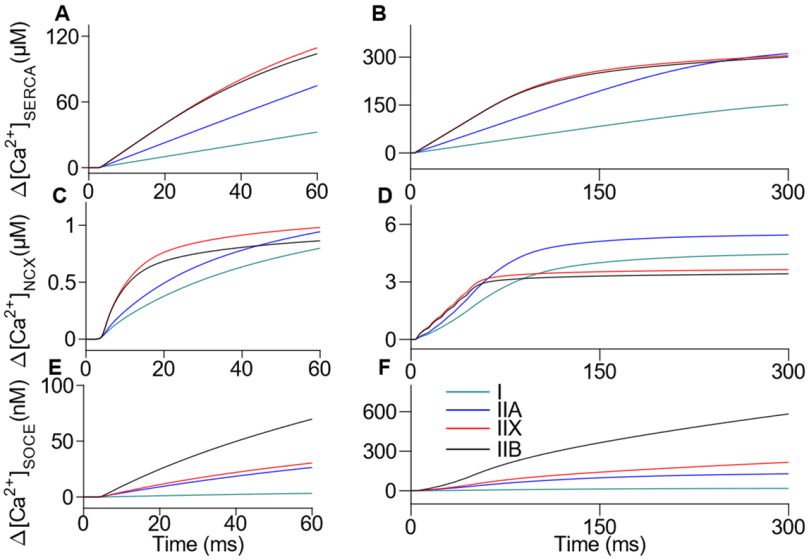

Figure 4. Simulation of kinetics of Ca^{2+} reuptake by the SR, and movement across the sarcolemma during single and tetanic Ca^{2+} transients in the continuum of fiber types. The $[Ca^{2+}]$ released is recaptured from the sarcoplasm to the SR by the SERCA (**A**,**B**), extruded from the sarcoplasm to the extracellular space through the NCX (**C**,**D**), and returned from the extracellular space to the sarcoplasm through the SOCE (**E**,**F**) in single (left column) and tetanic (right column) transients.

Table 1. List of parameters used for the multi-compartment model simulations of Ca^{2+} transients in skeletal muscle fiber types I, IIA, IIX, and IIB [a].

Parameter	Description	Fiber Type		References
		IIA, IIX, and IIB	I	
Sarcomeric volumes				
V_{SR}	Fiber volume occupied by the SR	5.5%	2.9%	[18]
$V_{T\text{-}tubule}$	Fiber volume occupied by the T-tubule	0.4%	0.2%	[18]
V_{mito}	Fiber volume occupied by MITO	8.5%	15.4%	[19]
V_{MS}	Fiber volume occupied by the MS	75%	81%	[20]
V_{sarc^*}	Fiber volume occupied by the sarcoplasm	85.6%	81.5%	(Present study)
Concentrations				
$[Ca^{2+}]_{rest,sarc}$	Resting free Ca^{2+} in sarcoplasm	106 nM	106 nM	[21]
$[Ca^{2+}]_{rest,SR}$	Resting free Ca^{2+} in SR	1.01 mM	1.14 mM	[22]
$[Mg^{2+}]_{rest,sarc}$	Resting free Mg^{2+} in sarcoplasm	0.78 mM	0.78 mM	[23]
$[Mg^{2+}]_T$	Total $[Mg^{2+}]$	3300 μM	3300 μM	[24]
$[Na^+]_{sarc}$	Sarcoplasmic $[Na^+]$	10 mM	10 mM	[25]
$[Na^+]_{mito}$	Mitochondrial $[Na^+]$	5 mM	5 mM	[26]
$[Na^+]_{extra}$	Extracellular $[Na^+]$	140 mM	140 mM	[25]
$[Ca^{2+}]_{extra}$	Extracellular $[Ca^{2+}]$	1 mM	1 mM	[25]
$[Tn]_T$	Total [Tn]	240 μM	120 μM	[13]
$[TNS]_T$	Total [TNS]	240 μM	240 μM	[13]
$[PV]_T$	Total [PV]	1900–60 μM	6 μM	[7,9,27]
$[ATP]_T$	Total [ATP]	8 mM	5 mM	[28]
$[CSQ]_T$	Total [CSQ]	46 mM	23 mM	[27]
$[B]_T$	Total [B]	20 μM	20 μM	[14]
SERCA				
V_{SERCA}	Maximum flux rate for SERCA	2.5–1.4 μM ms^{-1}	0.6 μM ms^{-1}	(Present study)
K_{SERCA}	SERCA half-maximum pump $[Ca^{2+}]$	0.44 μM	0.38 μM	[29]
h_{SERCA}	SERCA Hill coefficient	2.1	2.2	[29]

Table 1. *Cont.*

Parameter	Description	Fiber Type		References
		IIA, IIX, and IIB	I	
	MCU			
V_{MCU}	Maximum flux rate MCU	18.2 μM s^{-1}	74.3 μM s^{-1}	[13,16] and (Present study)
K_{MCU}	MCU half-maximum pump [Ca^{2+}]	1.2 μM	1.97 μM	[30]
h_{MCU}	MCU Hill coefficient	2	3.5	[30]
	NCE			
V_{NCE}	Maximum flux rate NCE	2.25 μM s^{-1}	9.19 μM s^{-1}	(Present study)
$K_{NCE,Ca^{2+}}$	Ca^{2+} binding constant of NCE	1.1 mM	1.1 mM	[14]
$K_{NCE,Na^{+}}$	Na^{+} binding constant of NCE	8.2 mM	8.2 mM	[31]
$\Delta\Psi_{m,mito}$	Mitochondrial membrane potential	190 mV	190 mV	[31]
	NCX			
V_{NCX}	Maximum flux rate NCX	214.5–120.1 μM s^{-1}	93.2 μM s^{-1}	(Present study)
$K_{NCX,Ca^{2+}}$	Ca^{2+} binding constant of NCX	140 μM	130 μM	[32]
$K_{NCX,Na^{+}}$	Na^{+} binding constant of NCX	14 mM	11 mM	[32]
$\Delta\Psi_m$	Sarcolemmal membrane potential	80 mV	80 mV	[25]
	SOCE			
V_{SOCE}	Maximum flux rate for SOCE	35–19 μM s^{-1}	15 μM s^{-1}	[33] and (Present study)
K_{SOCE}	SOCE half-maximum pump [Ca^{2+}]	0.35 mM	0.35 mM	[33]
h_{SOCE}	SOCE Hill coefficient	4.7	4.7	[33]

*V_{sarc} was calculated as 100%-V_{SR}-$V_{T\text{-}tubule}$-V_{mito}.

[a] The concentrations of free Ca^{2+} in the sarcoplasm and of the binding sites Tn, PV, ATP, and dye are referred to the sarcoplasmic water volume. The free Ca^{2+} in the SR and CSQ are relative to the SR volume. The free Ca^{2+} in the MITO and B are relative to the MITO volume. When required, the vales of the parameters taken from the literature were adjusted to 22 °C. SR: sarcoplasmic reticulum. MITO: mitochondria. MS: myofibril space. Tn: troponin. TNS: troponin non-specific sites. PV: parvalbumin. ATP: adenosine triphosphate. CSQ: calsequestrin. B: total MITO buffers. SERCA: sarcoendoplasmic reticulum Ca^{2+} adenosine triphosphatase. MCU: mitochondrial Ca^{2+} uniporter. NCE: mitochondrial Na^{+}/Ca^{2+} exchanger. NCX: Na^{+}/Ca^{2+} exchanger. SOCE: store-operated Ca^{2+} entry. *V* indicates maximum capacity of the mechanism. *K* indicates the concentration which induces half-maximal activation of the mechanism.

Table 2. Estimated kinetic parameters of the Ca^{2+} release rate function [a].

Fiber Type	I	IIA	IIX	IIB
Peak amplitude (μM ms^{-1})	64.8	153.6	238.8	244.5
10–90% Rise time (ms)	1.7	1.2	1.2	1.2
Half-width (ms)	1.9	1.4	1.3	1.3
90–10% Decay time (ms)	2.4	1.8	1.5	1.5
f_{Rel} (2nd AP)	0.17	0.18	0.18	0.17
f_{Rel} (3rd AP)	0.10	0.11	0.17	0.15
f_{Rel} (4th AP)	0.10	0.11	0.16	0.15
f_{Rel} (5th AP)	0.10	0.10	0.15	0.14

[a] f_{Rel} is the multiplication factor used in the second and subsequent action potentials (APs) to fit the measured peak amplitudes.

Table 3. Maximum [Ca^{2+}] variations reached during the simulated time intervals of single (60 ms) and tetanic (300 ms) Ca^{2+} transients of I, IIA, IIX, and IIB fiber types [a].

Fiber Type	I	IIA	IIX	IIB	I	IIA	IIX	IIB
	Single				Tetanic			
$\Delta[Ca^{2+}]$ (μM)	10.31	12.89	16.55	16.56	16.47	20.44	16.55	16.56
$[Ca^{2+}]_{SR}$ (mM)	0.93	0.7	0.65	0.64	0.87	0.64	0.57	0.54
$\Delta[Ca^{2+}]_{MITO}$ (μM)	0.93	0.42	0.25	0.23	1.9	0.83	0.58	0.56
Δ[CaB] (μM)	0.33	0.14	0.08	0.07	1.61	0.9	0.36	0.34

Table 3. *Cont.*

Fiber Type	I	IIA	IIX	IIB	I	IIA	IIX	IIB
	Single				Tetanic			
Δ[CaTn] (μM)	110.23	197.28	199.09	197.75	116.39	206.05	202.16	201.85
Δ[CaTNS] (μM)	10.17	8.79	6.84	6.52	32.15	25.99	14.42	13.92
Δ[CaPv] (μM)	0.78	7.63	141.78	170.66	1.76	16.27	247.96	304.5
Δ[CaATP] (μM)	23.34	46.61	59.75	59.79	37.16	73.65	59.75	59.79
Δ[CaDye] (μM)	3.23	4.02	5.14	5.14	5.11	6.31	5.14	5.14
$\Delta[Ca^{2+}]_T$ (μM)	133.69	238.93	325.8	343.28	168.29	300.92	441.78	489.53
$\Delta[Ca^{2+}]_{Rel}$ (μM)	145.48	254.58	346.68	363.71	213.43	381.58	558.4	606.1
Δ[CaCSQ] (mM)	−0.3	−1.29	−1.75	−1.85	−0.41	−1.7	−2.42	−2.69
$\Delta[Ca^{2+}]_{SERCA}$ (μM)	32.48	74.84	109.39	103.96	151.42	311.23	304.76	300.58
$\Delta[Ca^{2+}]_{NCX}$ (μM)	0.8	0.94	0.98	0.86	4.44	5.44	3.64	3.42
$\Delta[Ca^{2+}]_{SOCE}$ (nM)	3.29	26.39	30.44	69.73	18	129	215.9	582.63

[a] Abbreviations as in Table 1.

3. Discussion

The main findings of the present work were: (i) during a single twitch, the sarcoplasmic peak [Ca^{2+}] for fibers type IIB and IIX is between 15–25 μM, and for fibers type I and IIA reaches 6–12 μM, (ii) both the pattern of change and the peak concentrations of the Ca^{2+}-bound species in the sarcomere, the sarcolemma, and inside the SR showed the order IIB ≥ IIX > IIA > I, (iii) the mitochondrial peak [Ca^{2+}] and the MITO buffers saturation showed the pattern I >> IIA >> IIX ≥ IIB.

Previous models of mammalian ECC were affected by either uncertainty in the classification of fiber types, unreliable kinetics of the raw Ca^{2+} signals due to the use of slow Ca^{2+} dyes, or the lack of information about the role of several intracellular compartments in Ca^{2+} handling. To overcome these limitations, we based our model on the first calibration of Ca^{2+} transients of the four main fiber types found in mammals, obtained using the fast Ca^{2+} dye Mag-Fluo-4, and integrated new information gathered on MITO, SR, NCX, and SOCE, along basic knowledge on sarcoplasmic Ca^{2+} movements and buffering.

3.1. A Model which Includes Four Fiber Types

Preceding models addressed ECC in one or two fiber types, mainly as most previous functional and biochemical information came from a dichotomic approach of muscle fibers: either slow vs. fast, or type I vs. type II [13,14,16,34–37]. Additionally, simulations that have recently become spatially and mathematically more complex have remained biochemically oversimplified [38,39]. By taking Ca^{2+} transients obtained in molecularly typed fibers covering the whole spectra from I to IIB as experimental source, our model adds novel information on the ECC-fiber type relationships.

The fact that molecular and biochemical differences (i.e., isoforms and their biochemical properties) underlie the differences in ECC among fiber types has been described in detail elsewhere and we refer the readers to those papers [1,6,40].

However, there is still a lack of molecular and biochemical information, particularly for fibers type IIA and IIX. Our adjustments and results for these two types of fibers seem reliable as most values obtained laid between those of fibers type I and IIB. This agrees with the fact that fibers IIA and IIX showed kinetics of the Ca^{2+} transients, Ca^{2+} sensitivity, and other dynamic properties which are mostly intermediate between I and IIB [6,40–42]. Together, this confirms that most values of molecular, biochemical, and physiological parameters follow a continuum from I, to IIA, to IIX, to IIB.

3.2. [Ca^{2+}] Kinetics with a Fast Ca^{2+} Dye

The Ca^{2+} transients modeled in the present study were obtained with the fast Ca^{2+} dye Mag-Fluo-4. Two issues with quantitative impact on the results deserve attention: the biochemical properties of the dye and its loading conditions.

This dye has a 2:1 Mag-Fluo-4–Ca^{2+} binding stoichiometry, with an in situ K_d of 1.652×10^5 μM^2 [17]. This explains why it can reliably track the Ca^{2+} transients even in the fastest types, i.e., IIB, demonstrate subtle differences among all four fiber types and resolve every peak in a tetanic transient, being a trustable source for the model. On the other hand, as the fibers typically have ~200 μM of Mag-Fluo-4 [17], we found that less than ~3% of the dye is bound to Ca^{2+}.

The very low affinity of the dye and the lack of saturation confer Mag-Fluo-4 the ability to determine a trustable peak sarcoplasmic [Ca^{2+}]. Our results with Mag-Fluo-4 (calibration performed in the present study and [17]) join those with Mag-Fura-2 [16,35] which show that the peak [Ca^{2+}] in fast fibers IIX or IIB is typically between 15 and 25 μM in mammalian skeletal muscle (16–22 °C). The numbers for type I and IIA fibers also agree with a study reporting peak Ca^{2+} for soleus slow fibers [13]. That work, however, may have really used type I and IIA fibers, as the periphery of the soleus muscles of mouse used in the experiments have both types of fibers evenly distributed, as we have verified using specific antibodies and confocal microscopy (not shown). In conclusion, that paper and our results agree in that peak [Ca^{2+}] for fibers types I and IIA is between 6 and 12 μM [13]. The above numbers are one order of magnitude higher than those reported with slow dyes [14,33,43,44]. This fact may, for instance, reduce the estimated maximum rate of Ca^{2+} flux during SOCE or excitation-coupled Ca^{2+} entry (ECCE) activations [33,45], as this value depends on the driving force for Ca^{2+} [46], which in turn is reduced if sarcoplasmic [Ca^{2+}] is raised. Trustable peak sarcoplasmic [Ca^{2+}] also permits a better quantitation of the chemical species involved in ECC ([CaTn], [CaTNS], [CaPV], [CaATP], [CaDye], free [Ca^{2+}], etc.), including peak [Ca^{2+}] inside compartments such as MITO.

3.3. Comprehensive Integration of Mechanisms Involved in Ca^{2+} Handling: Sarcoplasm, SR, MITO, NCX and SOCE

The ECC is becoming more complex [1] and experimentally addressing some questions is challenging. For instance, important papers have investigated Ca^{2+} kinetics in MITO and SR, as well as SOCE function in fast fibers [33,47,48], but differences among all fiber types are infrequently [12] or never studied. The mathematical model presented here helps address these limitations.

The peak flux differences found in the release rate are consistent with the two- to ten-fold higher content of the ryanodine receptor (RyR) in the fastest fibers, compared to the other fibers [6,49–51]. The comparable values of half-width and rise time in all fiber types can be explained as all fiber types share the RyR1 isoform [52].

Upon release, Ca^{2+} has multiple fates: (i) binds to classical sarcoplasmic buffers such as PV, Tn, TNS, ATP, and the dye; (ii) enters into MITO and SR, or (iii) is recycled through the NCX and SOCE mechanisms [1].

In fast fibers (16–22 °C), [CaTn] has ranged from 80 μM [27] to around 240 μM [16,39], being ~199 μM for IIA, IIX, and IIB in the present study, within 7 ms from the beginning of the release of Ca^{2+}. Slow fibers gave values of 85 μM [13] and ~110 μM (fibers type I in the present study) within 15 ms. Different reaction rate constants arising from temperature corrections, our larger SERCA capacity, as well as the inclusion of MITO and SOCE, explain why the peak [CaTn] is somewhat lower in the fast fibers in our model than in the model of Baylor and Hollingworth (2007) [16]. The TNS peaked 31 μM during a train of APs in slow fiber types after 200 ms [13], and in the present work, such as with Tn, have peaked below, being 22 μM. Specifically in type IIX and IIB fibers, which have a higher quantity of PV, their influence is reduced, as the binding and unbinding rates are similar to those of PV.

The peak concentration of [CaPV] in fast fibers has ranged from 90 μM [27] to 120 μM [16], close to the 116–142 μM for IIX and IIB found in the present study, after 25 ms of Ca^{2+} release. Slow fibers are devoid of PV [13], or very low values have been measured in fibers type I and IIA in murines [53,54], justifying the values found (~0.5-5 μM) here. Then, the continuum of [CaPV] in I, IIA, IIX, and IIB fibers followed the order IIB > IIX >> IIA > I.

The peak [CaATP] we found for fibers IIX and IIB coincides with the values reported previously for fast fibers, i.e., 60 μM [27] and ~70 μM [16]. In all cases, the peak was within 6 ms from the release. In type I fibers, we report a value of 23 μM, with IIA being an intermediate. Then, the continuum of [CaATP] in all fibers was IIB = IIX > IIA > I.

The [CaDye] concentration reached a peak at around 22 μM [16] or 5 μM (IIB, present study) for fast fibers, indicating far-from-saturation conditions and likely not affecting Ca^{2+} release. Variations depend on differences in loading conditions used by the researchers in different laboratories. The value found for type I fibers in the present study was 3 μM. The order resembled that of the peak [Ca^{2+}] in the sarcoplasm and the Ca^{2+}-ATP reaction.

Peak change in [Ca^{2+}] inside MITO was reported to be 0.35 μM for a single twitch in fast fibers in Marcucci et al. (2018) [14]. The peak [Ca^{2+}] was ~0.25 μM in our results for fibers type IIX and IIB, about 25 ms after Ca^{2+} release. This concentration is similar to that obtained experimentally in fast mouse fibers [47]. Somewhat later, [Ca^{2+}] peaked inside MITO in type I fibers, reaching a value of 0.9 μM. This delay likely reflects Ca^{2+} diffusion into MITO, as measured in mouse using genetically encoded sensors [55]. Notably, the peak [Ca^{2+}] was far higher in I than in II, likely as the MCU of slow fibers has more capacity than that of the fast fibers [30], with no difference in the properties of the NCE, allowing more Ca^{2+} to accumulate inside MITO of fibers type I. Additionally, in fibers type I, the lower amount of PV compared to II allows more Ca^{2+} free to diffuse into MITO. For fibers IIA, their intermediate amount of Ca^{2+} released, along with their intermediate amount of PV and SERCA content may explain their midsize value of Ca^{2+} inside MITO. According to their peak amplitude, Ca^{2+} transients in MITO can be ordered as I >> IIA >> IIX $\geq$ IIB.

Previous works have estimated the total concentration of MITO buffers [B]. From the simulated analysis of the total [B] in cardiac muscle fibers performed in [56], a value of 2 μM was found to be optimal. In the work of Marcucci et al. (2018) [14] for skeletal muscle fibers a larger buffer concentration of 20 μM was also tested. In the present study, a value of 20 μM was used. A sizeable total [B] inside MITO is expected in order to deal with the larger and faster amounts of Ca^{2+} released in skeletal compared to cardiac muscle, and to explain the slowing of decay of the Ca^{2+} transients when the MITO uptake is blunted [12,47]. However, well calibrated, high resolution, experimental measurements of MITO Ca^{2+} buffering and kinetics are still required to reach an accurate estimate of the total [B] and [Ca^{2+}] inside MITO in skeletal muscle fibers.

Ca^{2+} pumped by the SERCA was estimated to be 1.5–3.5 μM in fast fibers [16], but amounted up to ~50 μM for IIX fibers in our model, after 25 ms. In slow fibers, a value somewhat below 1 μM was reported [13] at the same time (50 ms), but we found ~15 μM for type I. The differences between models can be explained due to temperature, as well as half-width differences in the recordings that fed the simulation. According to the intermediate kinetics of the decay phase of the Ca^{2+} transients in fibers IIA, as well as our previous discussion, midsize values for IIA were expected. The difference of Ca^{2+} pumped by SERCA 50 ms after Ca^{2+} release was IIB = IIX >> IIA >> I. The total capacity of Ca^{2+} extrusion by the NCX in fibers type IIB, IIX, and IIA was only 1.1—1.3 times higher than in I, suggesting that the larger amount of NCX1 in fibers type I is balanced by the larger capacity of the NCX3 present in fibers type II. The Ca^{2+} extruded by the t-system seems to be immediately recycled and has been called a counter-flux [5]. Our results confirmed that SOCE is quantitatively small in skeletal muscle [33,46], and it is difficult to speculate on the importance of the minor differences among fibers. More robust experimental data should be gathered before a conclusion about this issue can be stated.

3.4. Final Remarks

Although the above analyses give averages of peak sarcoplasmic/compartments [Ca^{2+}], spatially refined models for fast fibers have shown up to a 20-fold gradient in the sarcoplasmic [Ca^{2+}], depending on the distance of a subcellular region from the Ca^{2+} release units [13,16,39]. This phenomenon is also expected to apply to all fiber types, but the magnitude of those gradients inside the fibers was not explored in the present study.

Single-compartment simulations are expected to have errors associated with an inability to estimate local gradients in $[Ca^{2+}]$ and in the $[Ca^{2+}]$ bound to the binding sites. In the present study, the SOCE flux is associated with changes in $[Ca^{2+}]$ in the SR compartment. However, Ca^{2+} gradients in the SR have been measured during ECC and the Ca^{2+} levels decrease more rapidly in the terminal cisternae than in other regions of the SR [57]. Therefore, a model that considers the gradients in the SR would allow a more accurate estimate of the amount of Ca^{2+} entered by the SOCE.

Additionally, as our Ca^{2+}-bound chemical species had higher concentrations than those recently estimated, the thermal changes associated with ECC in mammalian muscle should be higher than proposed [27]. Our model may be a source to build a more complete model on thermal changes in all fiber types during single and tetanic stimulation.

4. Materials and Methods

4.1. Experimental Single and Tetanic Ca^{2+} Transients

Typical fluorescence experimental recordings (F) of single Ca^{2+} transients of fiber types I, IIA, IIX, and IIB were taken from [6]. Tetanic Ca^{2+} transients (100 Hz) of types I and IIB fibers were taken from [12]. The tetanic Ca^{2+} transient of IIA and IIX fibers were simulated assuming that they share morphology with I and IIB fibers, respectively, as published [6,12]. In all cases the signals were obtained with Mag-Fluo-4 in electrically stimulated isolated fibers from mouse muscles. Fibers were classified based on myosin heavy chain determination as detailed described in the above references. The conversion of F of single and tetanic experimental recordings to $[Ca^{2+}]$ was performed according to the calibration method and the value parameters presented in [17]. Briefly, $[Ca^{2+}]$ was calculated using the expression:

$$\left[Ca^{2+}\right] = \frac{K_d}{[D]_T} \frac{(F - F_{min})(F_{max} - F_{min})}{2(F_{max} - F)^2} \quad (1)$$

where F_{max} and F_{min} are the maximum and minimum fluorescences (150.9 A.U and 0.14 A.U) respectively, K_d is the in situ dissociation constant of Mag-Fluo-4 (1.652×10^5 μM^2), and $[D]_T$ is the total dye concentration (229.1 μM), at 20 °C. As the experimental Ca^{2+} transients that feed the model were acquired between 21–23 °C, no temperature corrections were performed in the calibration parameters.

4.2. Model Description

The rate of change of free $[Ca^{2+}]$ was described in three compartments (SR, sarcoplasm, and MITO) with a system of differential equations. The rate of change of $[Ca^{2+}]$ with respect to time in the SR was determined by

$$\frac{d\left[Ca^{2+}\right]_{SR}}{dt} = -J_{Rel} + J_{SERCA} - F\left(\left[Ca^{2+}\right]_{SR}, CSQ\right) \quad (2)$$

where J_{Rel} is the release rate flux, J_{SERCA} is the SERCA flux, and F the reaction rate of Ca^{2+} in the SR with calsequestrin (CSQ). The rate of change of sarcoplasmic $[Ca^{2+}]$ was expressed as:

$$\frac{d\left[Ca^{2+}\right]}{dt} = J_{Rel} - J_{SERCA} - J_{NCX} - \frac{d\left[Ca^{2+}\right]_{MITO}}{dt} + J_{SOCE} - F\left(\left[Ca^{2+}\right]_{SR}, S\right) \quad (3)$$

where J_{NCX} is the NCX flux, $[Ca^{2+}]_{MITO}$ the mitochondrial $[Ca^{2+}]$, J_{SOCE} is the SOCE flux, and $F([Ca^{2+}], S)$ the reaction rate with the sarcoplasmic Ca^{2+} binding sites S. The change in time of $[Ca^{2+}]$ in the MITO was given by

$$\frac{d\left[Ca^{2+}\right]_{MITO}}{dt} = J_{MCU} - J_{NCE} - F\left(\left[Ca^{2+}\right]_{MITO}, B\right) \quad (4)$$

where J_{MCU} was the inflow through the MCU, J_{NCE} outflow through the NCE, and $F([Ca^{2+}]_{MITO}, B)$ the reaction rate with B. The B was 20 µM of binding sites, which react with Ca^{2+} [14].

The parameters that describe the J_{Rel}, and the values of maximum capacity of SERCA, NCX, NCE, and SOCE (V_{SERCA}, V_{NCX}, V_{NCE}, and V_{SOCE}), were fitted to the measured Ca^{2+} transients. All other values of the model were taken from the literature, and the specific references are given in Table 1 and Table S1.

4.2.1. Release Rate of Ca^{2+}

The J_{Rel} of Ca^{2+} from the SR in fast and slow fibers were estimated from measurements of sarcoplasmic Ca^{2+} transients obtained with Mag-Fluo-4 (Figure 1A), as previously done with Mag-Fura-2 [35]. This approximation assumes that Ca^{2+} and other chemical species that react with Ca^{2+} are uniformly distributed in the sarcoplasm, which is thus described as a single compartment. The time derivative of the total Ca^{2+} concentration in the sarcoplasm, $d[Ca]_T/dt$, is given by the sum of the inflows and outflows through the membrane. Therefore, from the sum of $d[Ca]_T/dt$ and outflows, we obtained the release rate of Ca^{2+}. A gaussian model was used to simulate the J_{Rel} elicited by a single AP:

$$J_{Rel}(t) = \sum_{j=1}^{M} f_{Rel,j} \sum_{i=1}^{N} R_i e^{-\left(\frac{(t-(j-1)T_2)-T_{1,i}}{\tau_i}\right)^2} \quad (5)$$

where N is the number of peaks used to fit the J_{Rel} produced by a single AP, R is the peak amplitude, T_i is the location in the time axis, and τ relates to the width of each peak. R, T, and τ were adjusted to fit the peak amplitude, half-width, rise time, and decay time of the release rate of Ca^{2+} elicited by a single AP (Table 2). f_{Rel} is the multiplication factor used in the second and subsequent APs to fit the measured peaks amplitudes. M is the number of APs and T_2 of 10 ms is the time between stimulations.

4.2.2. Reaction of Ca^{2+} with Sarcomeric Buffers

The local reactions of Ca^{2+} with S of the chemical species in the compartments were described by the law of mass action,

$$F\left([Ca^{2+}], S\right) = k_{-}\left[SCa^{2+}\right] - k_{+}\left[Ca^{2+}\right][S] \quad (6)$$

with k_+ the binding rate constant, and k_- the unbinding rate constant. The interactions of Ca^{2+} and Mg^{2+} with the binding sites were described as reversible reactions. The reactions with ATP, B and CSQ were described as single reversible reactions. As Mg^{2+} competes with Ca^{2+} for the PV, their interactions are described with two simultaneous reversible reactions. Additionally, as recently described in Milán et al. (2021) [17], two molecules of the fluorescent indicator Mag-Fluo-4 (Dye) bind to one Ca^{2+}. The k_+ and k_- values associated with the ATP, Tn, and PV binding sites were taken from Baylor and Hollingworth (2007) [16] and Hollingworth et al. (2012) [13], CSQ from Barclay et al. (2021) [27], and B from Marcucci et al. (2018) [14]. A temperature of 22 °C and a Q_{10} of 2 were considered to adjust the reaction rates (Table S1). The resulting ordinary differential equations system was solved using the *ode15s* solver in MATLAB 2021b (MathWorks, Natick, MA, USA). The occupancy fraction of the binding sited at equilibrium were obtained from the simulated data.

4.2.3. Muscle Proteins Concentration

The Tn molecules concentration were 120 μM in all fiber types such as in Hollingworth et al. (2012) [13]. As each fast fiber Tn molecule has two Ca^{2+} binding sites and slow fiber molecules one, we thus assumed a concentration of 240 μM with positive cooperativity for IIA, IIX, and IIB fibers, and 120 μM for type I fibers. Additionally, as each Tn molecule has two non-specific sites (TNS) we considered concentrations of 240 μM for the binding sites of fast and slow fibers. As the Tn molecules are located in the myofibrillar space (MS), the average [Tn] and [TNS] in the sarcoplasm was rescaled by the occupation of the MS volume in the sarcoplasm (V_{MS} and V_{sarc} in Table 1).

The [PV] in the fastest fibers can achieve large concentrations, 1.5–1.9 mM [16,27]. We also considered that fibers type I have 300 times less [PV] [7], leading to 6 μM. Fibers IIA have a [PV] closer to fibers type I than type IIB, so we assumed 10 times more PV content in IIA than in I type [58], giving 60 μM, which is far lower than IIX and IIB, as expected. The ATP, Dye, CSQ, and B concentrations were listed in Table 1.

4.2.4. Reuptake Rate of Ca^{2+} by SERCA

The reuptake of Ca^{2+} by SERCA to the SR is described by the Michaelis–Menten kinetics and expressed as:

$$J_{SERCA} = V_{SERCA} \frac{\left[Ca^{2+}\right]^{h_{SERCA}}}{\left[Ca^{2+}\right]^{h_{SERCA}} + K_{SERCA}^{h_{SERCA}}} \quad (7)$$

where V_{SERCA} is the maximum flux rate, $[Ca^{2+}]$ is the Ca^{2+} concentration in the sarcoplasm, K_{SERCA} is the dissociation constant and h_{SERCA} the Hill coefficient. The SERCA isoform predominantly expressed in fast-twitch muscle fibers is the 1a, whereas in slow-twitch is the 2a [59]. Both have similar K_{SERCA} and h_{SERCA} [29], however different content of SR pump molecules [8], and thus V_{SERCA}. The V_{SERCA} was then adjusted to match the decay phase of the measured and simulated Ca^{2+} transients in all fiber types.

4.2.5. The Mitochondrial Ca^{2+} Uniporter (MCU) Inflow and the Sodium Ca^{2+} Exchanger (NCE) Outflow

The J_{MCU} was represented by a saturable first-order transporter, independent of the internal $[Ca^{2+}]_{MITO}$:

$$J_{MCU} = V_{MCU} \frac{\left[Ca^{2+}\right]^{h_{MCU}}}{\left[Ca^{2+}\right]^{h_{MCU}} + K_{MCU}^{h_{MCU}}} \quad (8)$$

where V_{MCU} is the maximum flux rate, $[Ca^{2+}]$ is the Ca^{2+} concentration in the sarcoplasm, and K_{MCU} is the $[Ca^{2+}]$ where the transport rate is half-maximum. V_{MCU} values were taken as 0.012 μM ms^{-1} in fast and 0.049 μM ms^{-1} in slow fibers at 16 °C [13,16], and adjusted considering a Q_{10} of 2.

The J_{NCE} was modelled with a stoichiometry of 3:1 and described with the following expression [31]:

$$J_{NCE} = V_{NCE} \left(\frac{e^{\frac{0.5\Delta\Psi_{m,mito}F}{RT}} \frac{\left[Na^+\right]^3 \left[Ca^{2+}\right]_{mito}}{K_{NCE,Na^+}^3 \cdot K_{NCE,Ca^{2+}}} - e^{-\frac{0.5\Delta\Psi_{m,mito}F}{RT}} \frac{\left[Na^+\right]_{mito}^3 \left[Ca^{2+}\right]}{K_{NCE,Na^+}^3 \cdot K_{NCE,Ca^{2+}}}}{1 + \frac{\left[Na^+\right]^3}{K_{NCE,Na^+}^3} + \frac{\left[Ca^{2+}\right]_{mito}}{K_{NCE,Ca^{2+}}} + \frac{\left[Na^+\right]^3 \left[Ca^{2+}\right]_{mito}}{K_{NCE,Na^+}^3 K_{NCE,Ca^{2+}}} + \frac{\left[Na^+\right]_{mito}^3}{K_{NCE,Na^+}^3} + \frac{\left[Ca^{2+}\right]}{K_{NCE,Ca^{2+}}} + \frac{\left[Na^+\right]_{mito}^3 \left[Ca^{2+}\right]}{K_{NCE,Na^+}^3 K_{NCE,Ca^{2+}}}} \right) \quad (9)$$

where $\Delta\Psi_{m,mito}$ is the mitochondrial membrane potential, V_{NCE} is the NCE activity, and $K_{NCE,Ca}{}^{2+}$ and $K_{NCE,Na}{}^{+}$ are the dissociation constants for the Ca^{2+} and Na^{2+} binding to the NCE, respectively. F, R, and T denote the Faraday constant, the ideal gas constant

and temperature, respectively. V_{NCE} was modulated in the fastest fibers to reproduce the speed of the $[Ca^{2+}]_{mito}$ decay phase, completed in a period of about 100 ms and measured during a single twitch, as in Rudolf et al. (2004) [55].

4.2.6. Ca^{2+} Flux through the NCX

To describe the sarcolemmal NCX, the same expression of the NCE, with stoichiometry of 3:1 was used, although with different simulated values. Reported Ca^{2+}-transport rate values for SERCA range from 10 (in membrane vesicles) to 13–14 nmol mg^{-1} min^{-1} (NCX3 and NCX1 isoforms, respectively) [60,61]. We assumed a maximum transfer rate (V_{NCX}) between 30 and 40% higher than that of SERCA. As the NCX is predominantly located in the T-tubule membrane [62], whereas the SERCA in the SR membrane, we thus rescaled V_{NCX} by a ratio (T-tubule membrane/SR membrane) of 0.066 and 0.111 in fast and slow fibers [20], i.e., between 214.5 and 120.1 μM s^{-1} for all fibers type II. In fibers type I we used 93.2 μM ms^{-1}. For $K_{NCX,Ca}{}^{2+}$ and $K_{NCX,Na}{}^{+}$, we, respectively took values of 140 μM and 14 mM in fast fibers, and 130 μM and 11 mM in slow fibers [32].

4.2.7. The Effect of Store-operated Ca^{2+} Entry (SOCE)

We described the flux, J_{SOCE}, as a fraction, P_{SOCE}, of a given maximum value, and V_{SOCE} as J_{SOCE}= V_{SOCE} P_{SOCE} [63]. As said, P_{SOCE} change as a function of the $[Ca^{2+}]$ in the SR, which can be described by the function:

$$P_{SOCE} = \frac{K_{SOCE}^{h_{SOCE}}}{\left[Ca^{2+}\right]_{SR}^{h_{SOCE}} + K_{SOCE}^{h_{SOCE}}} \quad (10)$$

where K_{SOCE} and h_{SOCE} are the Ca^{2+} dissociation constant of STIM1 (0.35 mM) and the Hill coefficient (4.7), respectively [33]. We assumed that the V_{SOCE} in the fastest IIB fibers achieved up to 35 μM s^{-1} [33]. Lower values were used for IIX, IIA, and I fibers.

5. Conclusions

Our mathematical, comprehensive model allows us to gain insight into the kinetics of the Ca^{2+} transients obtained with the fast Ca^{2+} dye Mag-Fluo-4, for the continuum of skeletal muscle fiber types. Sarcoplasmic peak $[Ca^{2+}]$ is one order of magnitude higher than reported with slow dyes. The magnitudes of change of the Ca^{2+}-bound forms of the Ca^{2+} buffers studied follow the order IIB $\geq$ IIX > IIA > I, except for mitochondrial peak $[Ca^{2+}]$ which showed the pattern I >> IIA >> IIX $\geq$ IIB. The kinetics for fibers IIA and IIX proved to be intermediate between I and IIB fibers, supporting dynamic data. The results may help better quantitate SOCE fluxes and thermal changes in mammalian fiber types in the future and support the use of fast Ca^{2+} dyes for most experimental approaches in skeletal muscle.

Supplementary Materials: The following are available online at https://www.mdpi.com/article/10.3390/ijms222212378/s1.

Author Contributions: All authors listed met the conditions required for full authorship. M.A.G. and J.C.C. designed the study and obtained the funding. O.A.R. prepared the mathematical model and M.A.G., J.C.C. and A.F.M. gave feedback. M.A.G., J.C.C. and O.A.R. analyzed the results. M.A.G. and J.C.C. wrote the first draft and all the authors reviewed and approved the final version. All authors have read and agreed to the published version of the manuscript.

Funding: This work was funded by the Committee of Research (CODI) of the University of Antioquia, Colombia (code 2015-7858) and the Planning Office of University of Antioquia (Project code E01708-K).

Institutional Review Board Statement: Not applicable.

Informed Consent Statement: Not applicable.

Data Availability Statement: The data presented in this study are available on request from the corresponding author.

Acknowledgments: We thank Jaime Ignacio Montoya for his support during the development of this investigation.

Conflicts of Interest: The authors declare no conflict of interest. The funders had no role in the design of the study; in the collection, analyses, or interpretation of data; in the writing of the manuscript, or in the decision to publish the results.

References

1. Calderón, J.C.; Bolaños, P.; Caputo, C. The excitation–contraction coupling mechanism in skeletal muscle. *Biophys. Rev.* **2014**, *6*, 133–160. [CrossRef] [PubMed]
2. Stiber, J.; Hawkins, A.; Zhang, Z.S.; Wang, S.; Burch, J.; Graham, V.; Ward, C.C.; Seth, M.; Finch, E.; Malouf, N.; et al. STIM1 signalling controls store-operated calcium entry required for development and contractile function in skeletal muscle. *Nat. Cell Biol.* **2008**, *10*, 688–697. [CrossRef]
3. Wei-LaPierre, L.; Carrell, E.M.; Boncompagni, S.; Protasi, F.; Dirksen, R.T. Orai1-dependent calcium entry promotes skeletal muscle growth and limits fatigue. *Nat. Commun.* **2013**, *4*, 2805. [CrossRef] [PubMed]
4. Protasi, F.; Pietrangelo, L.; Boncompagni, S. Calcium entry units (CEUs): Perspectives in skeletal muscle function and disease. *J. Muscle Res. Cell Motil.* **2021**, *42*, 233–249. [CrossRef] [PubMed]
5. Koenig, X.; Choi, R.H.; Launikonis, B.S. Store-operated Ca^{2+} entry is activated by every action potential in skeletal muscle. *Commun. Biol.* **2018**, *1*, 31. [CrossRef] [PubMed]
6. Calderón, J.C.; Bolaños, P.; Caputo, C. Myosin heavy chain isoform composition and Ca^{2+} transients in fibres from enzymatically dissociated murine soleus and extensor digitorum longus muscles. *J. Physiol.* **2010**, *588*, 267–279. [CrossRef]
7. Leberer, E.; Pette, D. Immunochemical quantification of sarcoplasmic reticulum Ca-ATPase, of calsequestrin and of parvalbumin in rabbit skeletal muscles of defined fiber composition. *Eur. J. Biochem.* **1986**, *156*, 489–496. [CrossRef]
8. Ferguson, D.G.; Franzini-Armstrong, C. The Ca^{2+} ATPase content of slow and fast twitch fibers of guinea pig. *Muscle Nerve* **1988**, *11*, 561–570. [CrossRef]
9. Heizmann, C.W. Parvalbumin, and intracellular calcium-binding protein; distribution, properties and possible roles in mammalian cells. *Experientia* **1984**, *40*, 910–921. [CrossRef]
10. Cannell, M.B.; Allen, D.G. Model of calcium movements during activation in the sarcomere of frog skeletal muscle. *Biophys. J.* **1984**, *45*, 913–925. [CrossRef]
11. Baylor, S.M.; Hollingworth, S. Model of Sarcomeric Ca^{2+} Movements, Including ATP Ca^{2+} Binding and Diffusion, during Activation of Frog Skeletal Muscle. *J. Gen. Physiol.* **1998**, *112*, 297–316. [CrossRef] [PubMed]
12. Calderón, J.C.; Bolaños, P.; Caputo, C. Tetanic Ca^{2+} transient differences between slow- and fast-twitch mouse skeletal muscle fibres: A comprehensive experimental approach. *J. Muscle Res. Cell Motil.* **2014**, *35*, 279–293. [CrossRef]
13. Hollingworth, S.; Kim, M.M.; Baylor, S.M. Measurement and simulation of myoplasmic calcium transients in mouse slow-twitch muscle fibres. *J. Physiol.* **2012**, *590*, 575–594. [CrossRef]
14. Marcucci, L.; Canato, M.; Protasi, F.; Stienen, G.J.M.; Reggiani, C. A 3D diffusional-compartmental model of the calcium dynamics in cytosol, sarcoplasmic reticulum and mitochondria of murine skeletal muscle fibers. *PLoS ONE* **2018**, *13*, e0201050. [CrossRef] [PubMed]
15. Baylor, S.M.; Hollingworth, S. Calcium indicators and calcium signalling in skeletal muscle fibres during excitation–contraction coupling. *Prog. Biophys. Mol. Biol.* **2011**, *105*, 162–179. [CrossRef] [PubMed]
16. Baylor, S.M.; Hollingworth, S. Simulation of Ca^{2+} movements within the sarcomere of fast-twitch mouse fibers stimulated by action potentials. *J. Gen. Physiol.* **2007**, *130*, 283–302. [CrossRef]
17. Milán, A.F.; Rincón, O.A.; Arango, L.B.; Reutovich, A.A.; Smith, G.L.; Giraldo, M.A.; Bou-Abdallah, F.; Calderón, J.C. Calibration of mammalian skeletal muscle Ca^{2+} transients recorded with the fast Ca^{2+} dye Mag-Fluo-4. *Biochim. Biophys. Acta-Gen. Subj.* **2021**, *1865*, 129939. [CrossRef]
18. Luff, A.R.; Atwood, H.L. Changes in the sarcoplasmic reticulum and transverse tubular system of fast and slow skeletal muscles of the mouse during postnatal development. *J. Cell Biol.* **1971**, *51*, 369–383. [CrossRef]
19. Chen, G.; Carroll, S.; Racay, P.; Dick, J.; Pette, D.; Traub, I.; Vrbova, G.; Eggli, P.; Celio, M.; Schwaller, B. Deficiency in parvalbumin increases fatigue resistance in fast-twitch muscle and upregulates mitochondria. *Am. J. Physiol. Physiol.* **2001**, *281*, C114–C122. [CrossRef]
20. Eisenberg, B.R. Quantitative Ultrastructure of Mammalian Skeletal Muscle. In *Comprehensive Physiology*; Wiley: Hoboken, NJ, USA, 1983; pp. 73–112.
21. Williams, D.A.; Head, S.I.; Bakker, A.J.; Stephenson, D.G. Resting calcium concentrations in isolated skeletal muscle fibres of dystrophic mice. *J. Physiol.* **1990**, *428*, 243–256. [CrossRef]
22. Fryer, M.W.; Stephenson, D.G. Total and sarcoplasmic reticulum calcium contents of skinned fibres from rat skeletal muscle. *J. Physiol.* **1996**, *493*, 357–370. [CrossRef]

23. Westerblad, H.; Allen, D.G. Myoplasmic free Mg^{2+} concentration during repetitive stimulation of single fibres from mouse skeletal muscle. *J. Physiol.* **1992**, *453*, 413–434. [CrossRef]
24. Westerblad, H.; Allen, D.G. The role of sarcoplasmic reticulum in relaxation of mouse muscle; effects of 2,5-di(tert-butyl)-1,4-benzohydroquinone. *J. Physiol.* **1994**, *474*, 291–301. [CrossRef]
25. Sperelakis, N. *Cell Physiology Source Book*; Elsevier Inc.: Amsterdam, The Netherlands, 2012; ISBN 9780123877383.
26. Boyman, L.; Chikando, A.C.; Williams, G.S.B.; Khairallah, R.J.; Kettlewell, S.; Ward, C.W.; Smith, G.L.; Kao, J.P.Y.; Lederer, W.J. Calcium movement in cardiac mitochondria. *Biophys. J.* **2014**, *107*, 1289–1301. [CrossRef]
27. Barclay, C.J.; Launikonis, B.S. Components of activation heat in skeletal muscle. *J. Muscle Res. Cell Motil.* **2021**, *42*. [CrossRef] [PubMed]
28. Kushmerick, M.J.; Moerland, T.S.; Wiseman, R.W. Mammalian skeletal muscle fibers distinguished by contents of phosphocreatine, ATP, and Pi. *Proc. Natl. Acad. Sci. USA* **1992**, *89*, 7521–7525. [CrossRef] [PubMed]
29. Lytton, J.; Westlin, M.; Burk, S.E.; Shull, G.E.; MacLennan, D.H. Functional comparisons between isoforms of the sarcoplasmic or endoplasmic reticulum family of calcium pumps. *J. Biol. Chem.* **1992**, *267*, 14483–14489. [CrossRef]
30. Sembrowich, W.L.; Quintinskie, J.J.; Li, G. Calcium uptake in mitochondria from different skeletal muscle types. *J. Appl. Physiol.* **1985**, *59*, 137–141. [CrossRef]
31. Dash, R.K.; Beard, D.A. Analysis of cardiac mitochondrial Na^{2+}-Ca^{2+} exchanger kinetics with a biophysical model of mitochondrial Ca^{2+} handing suggests a 3:1 stoichiometry. *J. Physiol.* **2008**, *586*, 3267–3285. [CrossRef] [PubMed]
32. Donoso, P.; Hidalgo, C. Sodium-calcium exchange in transverse tubules isolated from frog skeletal muscle. *Biochim. Biophys. Acta-Biomembr.* **1989**, *978*, 8–16. [CrossRef]
33. Koenig, X.; Choi, R.H.; Schicker, K.; Singh, D.P.; Hilber, K.; Launikonis, B.S. Mechanistic insights into store-operated Ca^{2+} entry during excitation-contraction coupling in skeletal muscle. *Biochim. Biophys. Acta-Mol. Cell Res.* **2019**, *1866*, 1239–1248. [CrossRef]
34. Gillis, J.M.; Thomason, D.; Lefèvre, J.; Kretsinger, R.H. Parvalbumins and muscle relaxation: A computer simulation study. *J. Muscle Res. Cell Motil.* **1982**, *3*, 377–398. [CrossRef]
35. Baylor, S.M.; Hollingworth, S. Sarcoplasmic reticulum calcium release compared in slow-twitch and fast-twitch fibres of mouse muscle. *J. Physiol.* **2003**, *551*, 125–138. [CrossRef]
36. Bakker, A.J.; Cully, T.R.; Wingate, C.D.; Barclay, C.J.; Launikonis, B.S. Doublet stimulation increases Ca^{2+} binding to troponin C to ensure rapid force development in skeletal muscle. *J. Gen. Physiol.* **2017**, *149*, 323–334. [CrossRef] [PubMed]
37. Senneff, S.; Lowery, M.M. Effects of extracellular potassium on calcium handling and force generation in a model of excitation-contraction coupling in skeletal muscle. *J. Theor. Biol.* **2021**, *519*, 110656. [CrossRef]
38. Wang, M.; Sun, J.; Yang, Q. Modeling and simulation of excitation-contraction coupling of fast-twitch skeletal muscle fibers. *Technol. Health Care* **2020**, *28*, 13–24. [CrossRef]
39. Holash, R.J.; MacIntosh, B.R. A stochastic simulation of skeletal muscle calcium transients in a structurally realistic sarcomere model using MCell. *PLoS Comput. Biol.* **2019**, *15*, e1006712. [CrossRef]
40. Bottinelli, R.; Reggiani, C. Human skeletal muscle fibres: Molecular and functional diversity. *Prog. Biophys. Mol. Biol.* **2000**, *73*, 195–262. [CrossRef]
41. Schiaffino, S.; Reggiani, C. Fiber Types in Mammalian Skeletal Muscles. *Physiol. Rev.* **2011**, *91*, 1447–1531. [CrossRef] [PubMed]
42. Schiaffino, S.; Gorza, L.; Sartore, S.; Saggin, L.; Ausoni, S.; Vianello, M.; Gundersen, K.; LØmo, T. Three myosin heavy chain isoforms in type 2 skeletal muscle fibres. *J. Muscle Res. Cell Motil.* **1989**, *10*, 197–205. [CrossRef] [PubMed]
43. Olsson, K.; Cheng, A.J.; Al-Ameri, M.; Wyckelsma, V.L.; Rullman, E.; Westerblad, H.; Lanner, J.T.; Gustafsson, T.; Bruton, J.D. Impaired sarcoplasmic reticulum Ca^{2+} release is the major cause of fatigue-induced force loss in intact single fibres from human intercostal muscle. *J. Physiol.* **2020**, *598*, 773–787. [CrossRef]
44. Weiss, N.; Andrianjafiniony, T.; Dupré-Aucouturier, S.; Pouvreau, S.; Desplanches, D.; Jacquemond, V. Altered myoplasmic Ca^{2+} handling in rat fast-twitch skeletal muscle fibres during disuse atrophy. *Pflugers Arch. Eur. J. Physiol.* **2010**, *459*, 631–644. [CrossRef] [PubMed]
45. Launikonis, B.S.; Stephenson, D.G.; Friedrich, O. Rapid Ca^{2+} flux through the transverse tubular membrane, activated by individual action potentials in mammalian skeletal muscle. *J. Physiol.* **2009**, *587*, 2299–2312. [CrossRef]
46. Launikonis, B.S.; Murphy, R.M.; Edwards, J.N. Toward the roles of store-operated Ca^{2+} entry in skeletal muscle. *Pflügers Arch.-Eur. J. Physiol.* **2010**, *460*, 813–823. [CrossRef]
47. Yi, J.; Ma, C.; Li, Y.; Weisleder, N.; Ríos, E.; Ma, J.; Zhou, J. Mitochondrial Calcium Uptake Regulates Rapid Calcium Transients in Skeletal Muscle during Excitation-Contraction (E-C) Coupling. *J. Biol. Chem.* **2011**, *286*, 32436–32443. [CrossRef]
48. Canato, M.; Scorzeto, M.; Giacomello, M.; Protasi, F.; Reggiani, C.; Stienen, G.J.M. Massive alterations of sarcoplasmic reticulum free calcium in skeletal muscle fibers lacking calsequestrin revealed by a genetically encoded probe. *Proc. Natl. Acad. Sci. USA* **2010**, *107*, 22326–22331. [CrossRef] [PubMed]
49. Appelt, D.; Buenviaje, B.; Champ, C.; Franzini-Armstrong, C. Quantitation of 'junctional feet' content in two types of muscle fiber from hind limb muscles of the rat. *Tissue Cell* **1989**, *21*, 783–794. [CrossRef]
50. Franzini-Armstrong, C.; Ferguson, D.G.; Champ, C. Discrimination between fast- and slow-twitch fibres of guinea pig skeletal muscle using the relative surface density of junctional transverse tubule membrane. *J. Muscle Res. Cell Motil.* **1988**, *9*, 403–414. [CrossRef]

51. Damiani, E.; Margreth, A. Characterization study of the ryanodine receptor and of calsequestrin isoforms of mammalian skeletal muscles in relation to fibre types. *J. Muscle Res. Cell Motil.* **1994**, *15*, 86–101. [CrossRef]
52. Lee, Y.S.; Ondrias, K.; Duhl, A.J.; Ehrlich, B.E.; Kim, D.H. Comparison of calcium release from sarcoplasmic reticulum of slow and fast twitch muscles. *J. Membr. Biol.* **1991**, *122*, 155–163. [CrossRef] [PubMed]
53. Ecob-Prince, M.S.; Leberer, E. Parvalbumin in mouse muscle in vivo and in vitro. *Differentiation* **1989**, *40*, 10–16. [CrossRef] [PubMed]
54. Gundersen, K.; Leberer, E.; Lømo, T.; Pette, D.; Staron, R.S. Fibre types, calcium-sequestering proteins and metabolic enzymes in denervated and chronically stimulated muscles of the rat. *J. Physiol.* **1988**, *398*, 177–189. [CrossRef]
55. Rudolf, R.; Mongillo, M.; Magalhaães, P.J.; Pozzan, T. In vivo monitoring of Ca^{2+} uptake into mitochondria of mouse skeletal muscle during contraction. *J. Cell Biol.* **2004**, *166*, 527–536. [CrossRef] [PubMed]
56. Wüst, R.C.I.; Helmes, M.; Martin, J.L.; van der Wardt, T.J.T.; Musters, R.J.P.; van der Velden, J.; Stienen, G.J.M. Rapid frequency-dependent changes in free mitochondrial calcium concentration in rat cardiac myocytes. *J. Physiol.* **2017**, *595*, 2001–2019. [CrossRef]
57. Reddish, F.N.; Miller, C.L.; Deng, X.; Dong, B.; Patel, A.A.; Ghane, M.A.; Mosca, B.; McBean, C.; Wu, S.; Solntsev, K.M.; et al. Rapid subcellular calcium responses and dynamics by calcium sensor G-CatchER^{+}. *iScience* **2021**, *24*, 102129. [CrossRef] [PubMed]
58. Heizmann, C.W.; Berchtold, M.W.; Rowlerson, A.M. Correlation of parvalbumin concentration with relaxation speed in mammalian muscles. *Proc. Natl. Acad. Sci. USA* **1982**, *79*, 7243–7247. [CrossRef]
59. Periasamy, M.; Kalyanasundaram, A. SERCA pump isoforms: Their role in calcium transport and disease. *Muscle Nerve* **2007**, *35*, 430–442. [CrossRef]
60. Linck, B.; Qiu, Z.; He, Z.; Tong, Q.; Hilgemann, D.W.; Philipson, K.D. Functional comparison of the three isoforms of the Na^{+}/Ca^{2+} exchanger (NCX1, NCX2, NCX3). *Am. J. Physiol. Physiol.* **1998**, *274*, C415–C423. [CrossRef] [PubMed]
61. Mickelson, J.R.; Beaudry, T.M.; Louis, C.F. Regulation of skeletal muscle sarcolemmal ATP-dependent calcium transport by calmodulin and cAMP-dependent protein kinase. *Arch. Biochem. Biophys.* **1985**, *242*, 127–136. [CrossRef]
62. Sacchetto, R.; Margreth, A.; Pelosi, M.; Carafoli, E. Colocalization of the Dihydropyridine Receptor, the Plasma-Membrane Calcium ATPase Isoform 1 and the Sodium/Calcium Exchanger to the Junctional-Membrane Domain of Transverse Tubules of Rabbit Skeletal Muscle. *Eur. J. Biochem.* **1996**, *237*, 483–488. [CrossRef] [PubMed]
63. Activation of Store-Operated Calcium Entry in Airway Smooth Muscle Cells: Insight from a Mathematical Model. Available online: https://journals.plos.org/plosone/article?id=10.1371/journal.pone.0069598 (accessed on 19 March 2021).